International Journal of Nanomedicine

Dovepress
open access to scientific and medical research

Open Access Full Text Article

ORIGINAL RESEARCH

Photocatalytic antibacterial application of zinc oxide nanoparticles and self-assembled networks under dual UV irradiation for enhanced disinfection

This article was published in the following Dove Medical Press journal:
International Journal of Nanomedicine

Su-Eon Jin[1]
Jun Eon Jin[2]
Woochul Hwang[3]
Seok Won Hong[4]

[1]Research Institute for Medical Sciences, College of Medicine, Inha University, Incheon 22212, Korea; [2]College of Electrical Engineering, Korea University, Seoul 02841, Korea; [3]ECOSET Co., Ltd., Ansan 15610, Korea; [4]Korea Institute of Science and Technology, Seoul 02792, Korea

Background: Zinc oxide (ZnO) nanoparticles and their networks have been developed for use in various applications such as gas sensors and semiconductors.

Aim: In this study, their antibacterial activity against *Escherichia coli* under dual ultraviolet (UV) irradiation for disinfection was investigated.

Materials and methods: ZnO nanoparticles were synthesized and immobilized onto silicon (Si) wafers by self-assembly. The physicochemical properties and antibacterial activity of ZnO nanoparticles and their networks were evaluated. Gene ontology was analyzed and toxicity levels were also monitored.

Results: Synthesized ZnO nanoparticles were spherical nanocrystals (<100 nm; Zn, 47%; O, 53%) that formed macro–mesoporous three-dimensional nanostructures on Si wafers in a concentration-dependent manner. ZnO nanoparticles and their networks on Si wafers had an excellent antibacterial activity against *E. coli* under dual UV irradiation (>3log CFU/mL). Specifically, arrayed ZnO nanoparticle networks showed superior activity compared with free synthesized ZnO nanoparticles. Oxidative stress-responsive proteins in *E. coli* were identified and categorized, which indicated antibacterial activity. Synthesized ZnO nanoparticles were less cytotoxic in HaCaT with an IC50 of 6.632 mg/mL, but phototoxic in Balb/c 3T3.

Conclusion: The results suggested that ZnO nanoparticles and their networks can be promising photocatalytic antibiotics for use in next-generation disinfection systems. Their application could also be extended to industrial and clinical use as effective and safe photocatalytic antibiotics.

Keywords: zinc oxide nanoparticles, immobilization, dual UV, antibacterial, disinfection, toxicity

Introduction

Zinc oxide (ZnO) nanoparticles have shown promise as an alternative to titanium oxide (TiO_2) nanoparticles in energy conservation and transfer applications such as batteries, solar cells, transistors, photocatalysis, purification, and biosensing.[1,2] Recently, metal oxide nanoparticles have been extensively studied as nanoantibiotics for enhanced disinfection, particularly for drug-resistant bacteria and parasites.[3,4] Under ultraviolet (UV) irradiation, these particles mediate oxidative stress in microorganisms.[5,6] Although ZnO is a Zn-based compound generally recognized as safe by the US Food and Drug Administration,[7,8] the safety of ZnO nanoparticles should be confirmed. Exposure risks to the environment and human health also need to be investigated and minimized.

ZnO nanoparticles are attractive potential broad-spectrum nanoantibiotics. ZnO nanoparticles and their nanoparticles adopted by other metal/metal oxides and other polymers have antimicrobial activity against *Escherichia coli*,[6,8–11] *Staphylococcus aureus*,[8–10] *Klebsiella pneumoniae*,[11] M13 bacteriophages,[6] and skin-specific

Correspondence: Su-Eon Jin
Research Institute for Medical Sciences, College of Medicine, Inha University, 100 Inha-ro, Michuhol-gu, Incheon 22212, Korea
Email jins@inha.ac.kr

submit your manuscript | www.dovepress.com
Dovepress
http://dx.doi.org/10.2147/IJN.S192277

pathogens[12] with/without UV irradiation. They also have antimicrobial activity against methicillin-resistant *S. aureus* based on modification of reactive oxygen species (ROS)-mediated pyridine synthesis and multiple metabolic pathways.[13] Therefore, engineered ZnO nanoparticles and their networks could be used to develop effective and safe antimicrobial agents.

Immobilization of nanoparticles on a solid plate has the advantage of eliminating the risk of nanoparticle exposure in unintended targets.[14–17] Specifically, nanofabrication by self-assembly is a valuable technique for developing three-dimensional nanostructures with smart properties for enhanced efficacy and safety.[18,19] Nanowires, nanocages, nanofilms, and nanosheets have been developed into revolutionary nanostructures.[20,21] ZnO nanoparticle aggregates and multilevel porous ZnO nanoparticle networks immobilized on solid plates can be effectively and safely applied for disinfection purposes based on their enhanced energy exchange and transfer.

In the present study, we hypothesized that ZnO nanoparticles and their three-dimensional networks attached to silicon (Si) wafers via self-assembly could have enhanced antibacterial activity against *E. coli* under dual UV irradiation (UV-A and UV-C). ZnO nanoparticles were thus synthesized and immobilized on Si wafers, and physicochemical characterization and antibacterial activity tests were performed. Cytotoxicity in HaCaT and ARPE-19 cells and phototoxicity in Balb/c 3T3 cells were also investigated. Nano-to-micro-ZnO (hybrid-ZnO) and nano-ZnO particles were used as conventional ZnO particle products.

Materials and methods

Chemicals

Hybrid- and nano-ZnO particles were purchased from Sigma (St Louis, MO, USA). Ethanol, hexane, zinc acetylacetonate hydrate, and oleylamine were also obtained from Sigma. All chemicals were of reagent grade without further purification. Deionized water was obtained using a Milli-Q water purification system (Millipore, Billerica, MA, USA).

Synthesis of ZnO nanoparticles

ZnO nanoparticles were synthesized from zinc acetylacetonate hydrate (0.2 g) and oleylamine (70%, 5 g). This mixture was heated at 80°C for 30 minutes under an argon atmosphere and then kept at 150°C for 1 hour. After cooling to room temperature, it was poured into 200 mL of ethanol to produce white precipitate. The precipitate was filtered, washed three times with ethanol, and dried. The removal of residual amines was confirmed by Fourier transform-infrared spectroscopy.

Nanofabrication by self-assembly

ZnO nanoparticles were arrayed on Si wafers (Semiroad, Inc., Paju, Kyunggi-do, Korea) to develop three-dimensional nanostructure networks. Si wafers were rinsed and residual solvents were removed. Nanoparticle dispersions in hexane were dropped onto the Si wafers as 0.05–1.0 mg of ZnO nanoparticles per unit Si wafer (0.5×0.5 cm^2). Then, the wafers were incubated at room temperature in the dark.

X-ray photoelectron spectroscopy (XPS)

Atomic composition was determined using XPS (K-Alpha, Thermo Fisher Scientific Inc., Waltham, MA, USA) with a source of monochromated Al K-alpha.

Field emission-scanning electron microscopy (FE-SEM) with energy-dispersive X-ray spectroscopy (EDS)

The morphology was monitored using FE-SEM (S-4300SE, Hitachi, Co. Ltd., Tokyo, Japan) operated at an acceleration voltage of 15.0 kV. Samples were investigated after platinum coating. Particle size distribution was analyzed using ImageJ (NIH). EDS analysis was also performed after particle surface scanning (20 runs) at 1,800× magnification. Samples used for EDS analyses were examined before platinum coating.

Field emission-transmission electron microscopy (FE-TEM)

The crystal shape and size were observed using FE-TEM (JEM-2100F, Jeol, Co. Ltd., Peabody, MA, USA) at an acceleration voltage of 100 kV. Nanoparticles were dispersed in hexane and dropped onto a copper grid (300 meshes). They were then investigated after drying in the dark. FE-TEM images were analyzed using Gatan Microscopy Suite Software (Gatan, Inc., Pleasanton, CA, USA).

Atomic force microscopy (AFM)

The surface topology and phase were determined using AFM (Nanoscope Multimode IVa, Bruker, Billerica, MA, USA) in tapping mode. Images were analyzed using NanoScope software (5.31r1, Veeco Instruments, Inc., Plainview, NY, USA).

Collimated beam device (CBD)

A CBD was prepared using a dual UV lamp (85 cm in length) with both UV-A (315–400 nm) and UV-C (100–280 nm; ECOSET Co., Ltd., Ansan, Korea) connected to an electronic controller of 40 W/m^2, which can be adjusted to emit focused and narrow light.[6] The dual UV lamp was coated on half of the surface by length. The uncoated side of the UV lamp was used. UV intensity was measured at the Petri dish using a

spectrometer (Jaz System; Ocean Optics, Inc., Petaluma, CA, USA) with Spectra Suite software (Ocean Optics, Inc.). The UV dose (J/m^2) was calculated by multiplying the UV lamp intensity (W/m^2) by exposure time (s).

Antibacterial activity test against *E. coli*

E. coli (American Type Culture Collection, ATCC, Manassas, VA, USA) was used as a model microorganism. For particle effects, ZnO nanoparticles were dispersed in water at 0.05–1.0 mg/mL. They were irradiated once for 30 seconds while incubated with *E. coli* (2.0×10^4 CFU) for 5 minutes. Tests were performed in triplicate. Then, samples were collected, diluted, and added to each Petrifilm™ (3M, Maplewood, MN, USA). The films were incubated in the dark at 35°C overnight and colonies were counted using ImageJ (NIH) after obtaining images. Water samples were also collected from three facilities with sterile 1-L-sized bottles to monitor the antibacterial activity of dual UV-ZnO nanoparticle treatments against *E. coli*. These were stored at 4°C for 7 days, and antibacterial activity testing was performed. For the immobilized particle network on Si wafers (0, 0.05, 0.1, 0.5, and 1.0 mg/wafer), one piece of Si wafer was used for each Petri dish. *E. coli* (2.0×10^4 CFU) in water was poured into each Petri dish after fixing the Si wafer to the bottom. After dual UV irradiation (5 and 10 seconds), they were incubated in the dark (5 minutes and 2 hours). Then, each sample was handled as mentioned above.

Systems biology analysis

Gene ontology (GO) terms related to oxidative stress from metal oxides were analyzed for *E. coli* using EcoCyc (SRI International, Menlo Park, CA, USA).[22] Search results from the *E. coli* database (EcoCyc) were summarized based on the hierarchy of biological process groups. Members of GO terms were also listed.

Cytotoxicity testing

HaCaT (human keratinocyte, CLS Cell Lines Service GmbH, Eppelheim, Germany) and ARPE-19 (human retinal pigmented epithelial cell, ATCC) were cultured in DMEM and DMEM/F12 supplemented with 10% FBS (Thermo Fisher Scientific, Waltham, MA, USA) and 100 U of penicillin–streptomycin (Thermo Fisher Scientific), respectively. They were incubated at 37°C in a CO_2 incubator with 5% CO_2 and appropriate humidity. HaCaT and ARPE-19 cells were seeded at 1.0×10^4 cells/well in 96-well plates. After 48-hour incubation, cells were treated with free nanoparticles in water at 0.01–10 mg/mL. After 48 and 72 hours of incubation, CellVia® (Young In Frontier Co. Ltd., Seoul, Korea) was diluted with each medium and applied to cells. After 4-hour incubation in a CO_2 incubator, absorbance was measured at 450 nm. The reference wavelength was 600 nm. Cell viability at concentration C was calculated by

$$\text{Cell viability (\%)} = \frac{\left(\text{Absorbance}_{450\text{ nm}} - \text{Absorbance}_{600\text{ nm}}\right)\text{ at } C\text{ mg/mL}}{\left(\text{Absorbance}_{450\text{ nm}} - \text{Absorbance}_{600\text{ nm}}\right)\text{ at 0 mg/mL}} \times 100$$

EC50 was also calculated using Excel software (2010 version, Microsoft, Redmond, WA, USA).

Phototoxicity testing

Balb/c 3T3 (mouse embryonic fibroblast, A31, ATCC) cells were cultured in DMEM (Thermo Fisher Scientific) with 10% newborn calf serum (Thermo Fisher Scientific) and 100 U of penicillin–streptomycin (Thermo Fisher Scientific), which were incubated at 37°C with 5% CO_2 and appropriate humidity. For tests, they were seeded at 1.0×10^3 cells/well in 96-well plates. After 48-hour incubation, cells were rinsed and incubated with Earle's balanced salt solution (EBSS, Thermo Fisher Scientific) for 1 hour. Then, they were treated with nanoparticles in EBSS (Thermo Fisher Scientific) at 0.001–1.0 mg/mL. One group was incubated under dual UV at room temperature for 30 minutes and the other group was incubated in the dark at room temperature for 30 minutes. After replacing the culture medium, cells were incubated overnight and the neutral red uptake testing was performed. Photo-irritation-factor (PIF) and mean photo effect (MPE) were calculated using Phototox software (ver 2.0, Bundesinstitut für Risikobewertung, Berlin, Germany). Substances were classified by PIF and MPE values: probably phototoxic ($2< \text{PIF} <5$; $0.1< \text{MPE} <0.15$) and phototoxic ($5< \text{PIF}$; $0.15< \text{MPE}$). Chlorpromazine was used as the control.

Statistical analysis

The results are expressed as the mean±SD. The statistical significance of the differences between groups was tested using the Student's t-test, with $p<0.05$ considered significant.

Results

Morphology, crystallinity, particle size distribution, and atomic composition

Synthesized ZnO nanoparticles generated spherical cluster shapes up to 3 μm (Figure 1A). Single ZnO nanoparticle was formed by uneven surface, which showed crystallinity with d-spacing of 0.265 nm for nanocrystal (002) (JCPDS 36-1451; Figure 1B). The average size was 48.3±3.5 nm in diameter with a narrow size distribution (Figure 1C). The aggregates generated a macro–mesoporous network based on interparticle interactions (Figure 1D). However, hybrid-ZnO particles were a

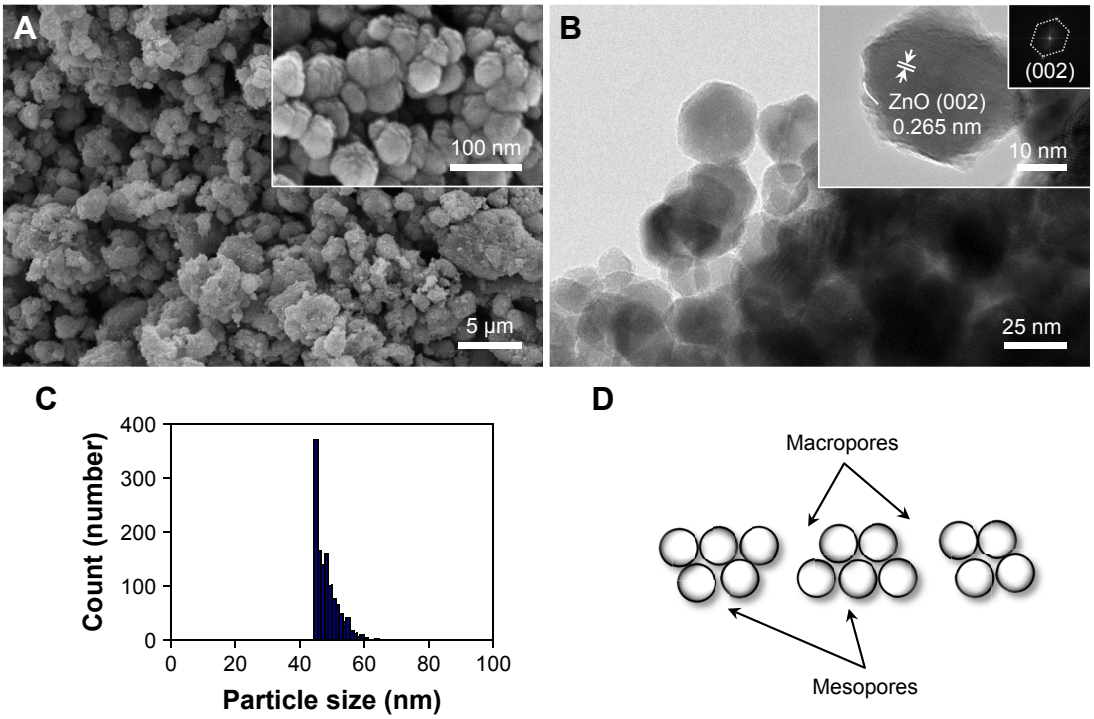

Figure 1 Synthesized ZnO nanoparticles: (**A**) FE-SEM images, (**B**) FE-TEM images with crystallinity and electron diffraction, (**C**) size distribution plot, and (**D**) schematic diagram of macro-mesopores.
Abbreviations: FE-SEM, field emission-scanning electron microscopy; FE-TEM, field emission-transmission electron microscopy; ZnO, zinc oxide.

mixture of needle, rod, and sphere-shaped particles of nanoscale to microscale size (Figure S1A and A′) and nano-ZnO particles had small rectangular bullet shapes (Figure S1B and B′). For atomic composition analysis, synthesized ZnO nanoparticles consisted of 47.38% Zn and 52.62% O (Table 1). Compared with synthesized ZnO nanoparticles, hybrid- and nano-ZnO particles had 44.8% and 48.16% Zn and 55.2% and 51.84% O, respectively. On XPS spectra, binding energy peaks of Zn2p were detected at 1,021 eV, and 1,044 eV for $Zn2p_{3/2}$ and $Zn2p_{1/2}$ (Figure S2). An O1s peak was also detected at 530 eV.

Nanostructure network generation of immobilized ZnO nanoparticles on Si wafers

Synthesized ZnO nanoparticles on Si wafers were in a highly ordered network with macro-mesopores (Figure 2) compared with hybrid- and nano-ZnO particles on the 0.5 mg/Si wafer (Figure S3). After simple dripping of a ZnO nanoparticle hexane suspension onto Si wafers, the patterned macropores of hemispherical and spherical ZnO nanoparticle aggregates were generated by gradual solvent evaporation, while mesopores in network were maintained (Figure 2A). As drop concentrations increased (0.05–1.0 mg/Si wafer), layer-by-layer structures in the ZnO nanoparticle network were produced after hexane evaporation (Figure 2B–Q). The atomic compositions of the aggregates on Si wafers were confirmed with EDS spectra (Figure 2E, I, M, and Q).

Table 1 Composition of ZnO particles

Binding energy peak	Atomic composition (%)		
	Hybrid-ZnO	Nano-ZnO	Synthesized ZnO
Zn2p	44.8	48.16	47.38
O1s	55.2	51.84	52.62

Abbreviation: ZnO, zinc oxide.

Arrayed ZnO nanoparticle interactions on Si wafers

Figure 3 shows the AFM topology and phase of immobilized ZnO nanoparticles on the Si wafers. Since ZnO nanoparticles at 0.05 mg/Si wafer were used, small ZnO nanoparticle aggregates were generated (0.2–0.3 to 2.3–2.6 μm in diameter) that did not form a hierarchically porous network. During aggregate formation (Figure 3A, white arrow), small ZnO nanoparticle clusters formed with mesopores and grew into large aggregates (>2 μm in diameter) with 353.06 nm roughness (Figure 3B). Small ZnO nanoparticle clusters (<1.0 μm in diameter) remained on the Si wafers (Figure 3C). From the phase results, hexagonal forms of ZnO nanoparticle aggregates were included in both the small and large

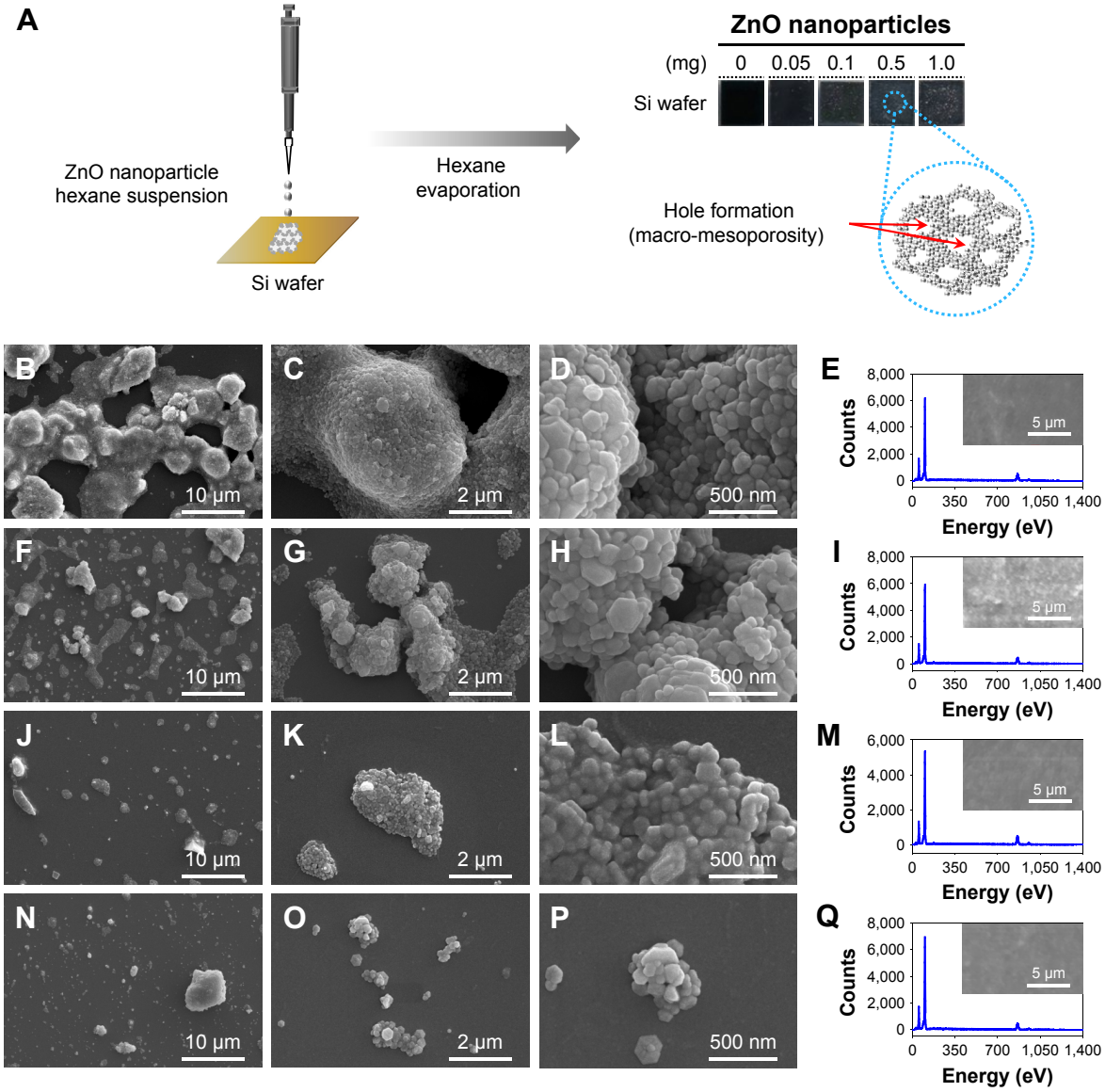

Figure 2 Arrayed ZnO nanoparticles on Si wafers.

Notes: (**A**) In situ array on an Si wafer and (**B**–**P**) FE-SEM images with EDS spectra. Synthesized ZnO nanoparticles were loaded at (**B**–**E**) 1.0, (**F**–**I**) 0.5, (**J**–**M**) 0.1, and (**N**–**Q**) 0.05 mg per unit Si wafer (0.5×0.5 cm^2). O at 53 eV; Zn at 103 eV, 864 eV, and 957 eV in EDS spectra. (**E**, **I**, **M**, and **Q**) Scanned images of ZnO nanoparticles on Si wafers were added onto EDS spectra.

Abbreviations: EDS, energy-dispersive X-ray spectroscopy; FE-SEM, field emission-scanning electron microscopy; Si, silicon; ZnO, zinc oxide.

aggregates (Figure 3D), which adopted a wurtzite crystal structure. The AFM results of ZnO nanoparticle aggregates on Si wafers are comparable to the FE-SEM results.

Dual UV irradiation

The average intensity level was 54.5±1.80 W/m^2 of the whole wavelength divided by 10.5±0.0330 W/m^2 of UV-A and 43.2±1.80 W/m^2 of UV-C (1:4.13 of UV-A to UV-C) (Figure 4). Half of the dual UV lamp by length was coated to block UV light scattering and to maximize the dual UV intensity to the uncoated side of lamp. A CBD was used to control the dual UV intensity at Petri dishes.

Antibacterial activity of dual UV-irradiated ZnO nanoparticles against *E. coli*

The dual UV-ZnO nanoparticle system had antibacterial activity against *E. coli* (Figure 5A), which was enhanced even at the lowest concentration (0.05 mg/mL) compared with UV alone. Hybrid-ZnO particles also offered excellent activity at the lowest concentration (0.05 mg/mL), whereas nano-ZnO particles showed considerable activity at the highest concentration (1.0 mg/mL). In a 100-fold dilution of *E. coli* (Figure 5B), 10 CFU/mL was detected without

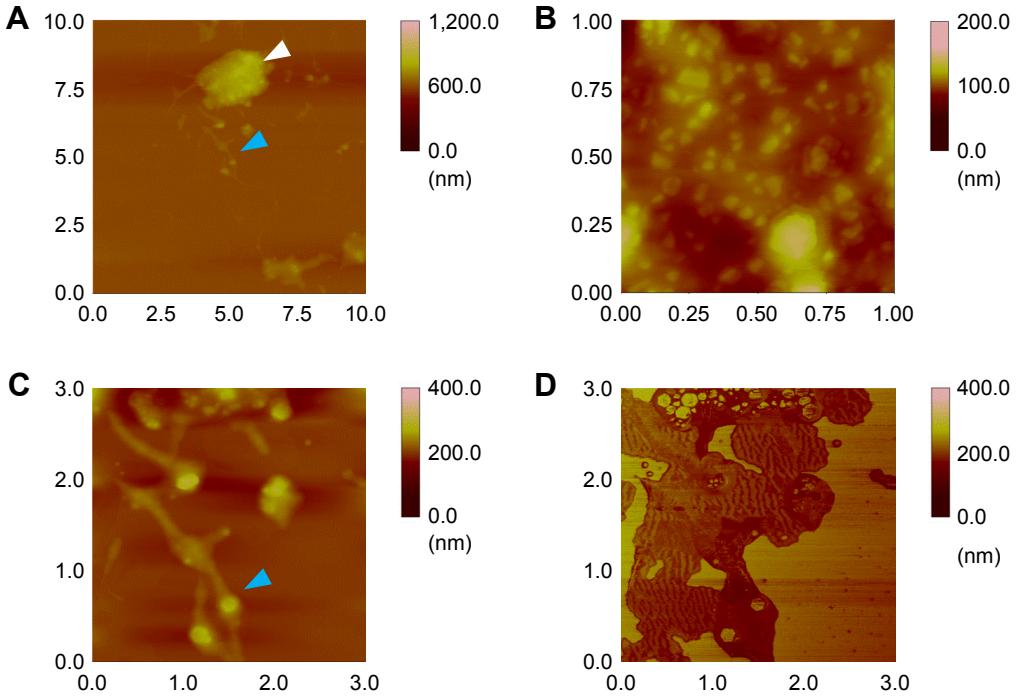

Figure 3 Synthesized ZnO nanoparticle interactions on Si wafers: (**A**–**C**) topology and (**D**) phase of AFM images at 0.05 mg/wafer.
Note: White and blue arrows represent the expanded areas to be confirmed.
Abbreviations: AFM, atomic force microscopy; ZnO, zinc oxide.

UV irradiation. After dual UV irradiation for 30 seconds, *E. coli* (7 CFU/mL) was still detected (Figure 5C). However, after dual UV-irradiated (30 seconds) ZnO nanoparticle (0.05 mg/mL, incubation for 5 minutes) treatment, no colonies were detected (Figure 5D). Their disinfection potential was also investigated in samples from L1, L2, and L3 facilities (Figure 5E–O). Colonies were too numerous to count in the L1 facility (Figure 5G) compared with the others

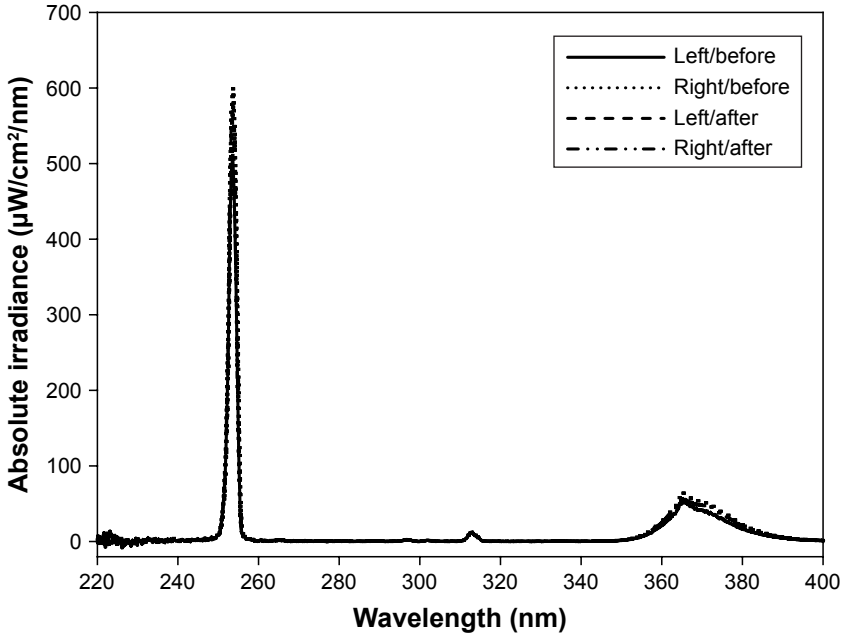

Figure 4 Dual UV spectra.
Notes: UV-A and UV-C intensities were maintained before and after antibacterial activity tests. Left and right represent the outputs for two-pathway UV irradiation in a CBD.
Abbreviations: CBD, collimated beam device; UV, ultraviolet.

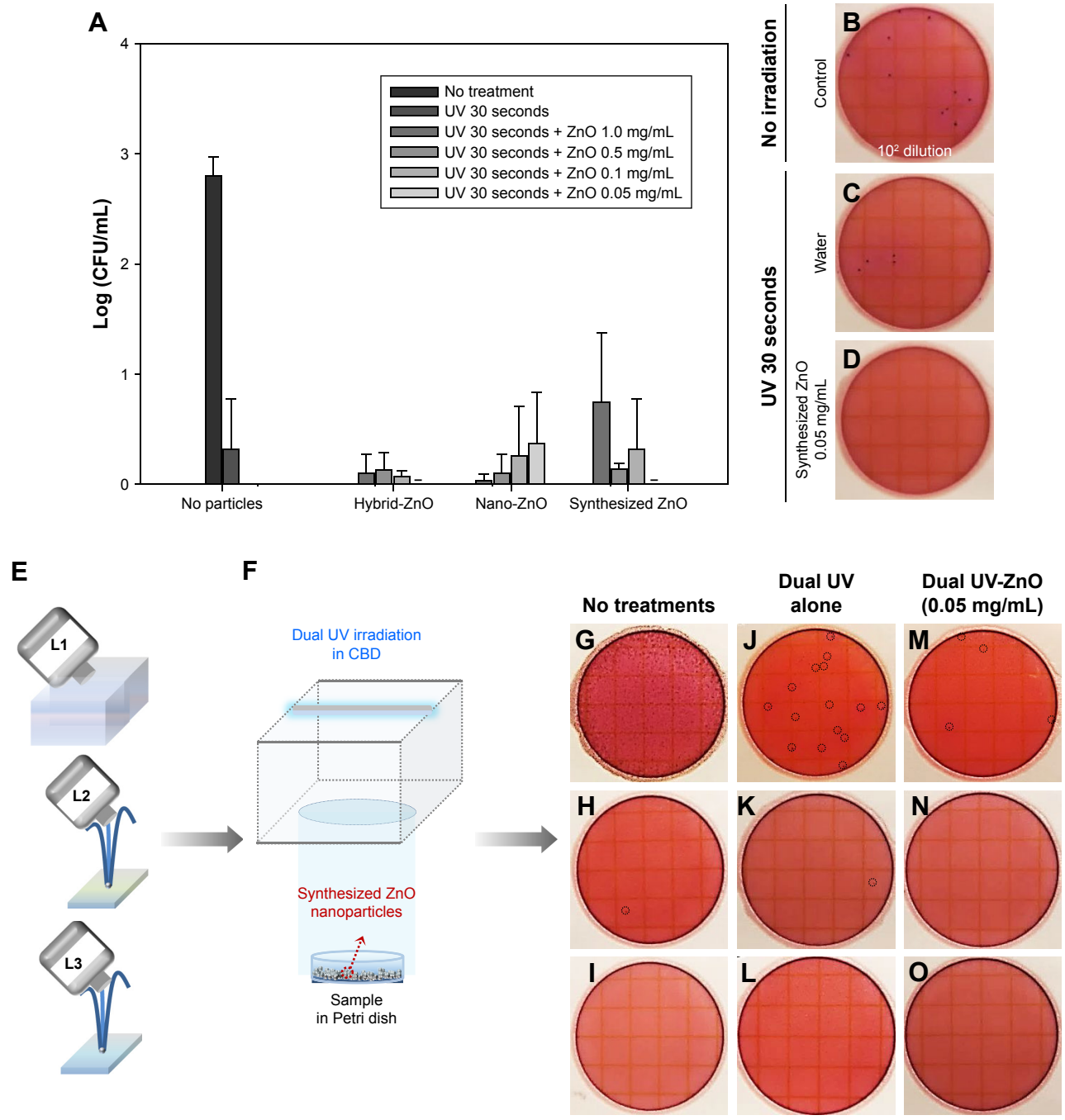

Figure 5 Antibacterial activity of the dual UV-irradiated ZnO nanoparticles against *Escherichia coli*.
Notes: (**A**) Plots of ZnO particle concentration *vs* log (CFU/mL). Representative plate images of (**B**) *E. coli* colonies (10^2 dilution) with no treatment, (**C**) *E. coli* colonies after dual UV irradiation alone (30 seconds), and (**D**) after dual UV-irradiated (30 seconds)-ZnO nanoparticle (0.05 mg/mL) treatment with a 5-minute incubation period. (**E**) Schematic diagram of water sampling from L1, L2, and L3 locations (a pool and two fountains) and (**F**) dual UV irradiation in a CBD with ZnO nanoparticle treatment. (**G**–**O**) Representative film images of samples from L1, L2, and L3 treated with/without dual UV-ZnO nanoparticles (**G**–**I**, no treatment; **J**–**L** dual UV irradiation for 30 seconds; **M**–**O**, dual UV [30 seconds]-ZnO nanoparticles [0.05 mg/mL, 5 minutes]). (**A**) – represents 'not detected'. (**J**, **M**, **H**, and **K**) Round dot circles represent *E. coli* colonies.
Abbreviations: CBD, collimated beam device; UV, ultraviolet; ZnO, zinc oxide.

(Figure 5H and I). The dual UV-irradiated ZnO nanoparticle system showed superior disinfection potential compared with UV alone (Figure 5J and M, round dot circles for *E. coli* colonies). No colonies were detected in the L3 facility (Figure 5I).

Antibacterial activity of dual UV-irradiated ZnO nanoparticles immobilized on Si wafers against *E. coli*

Figure 6 shows the antibacterial activity of ZnO nanoparticle-immobilized Si wafers against *E. coli*. Using these Si wafers

of arrayed ZnO nanoparticles, the UV irradiation time was set at 5 and 10 seconds. The UV exposure time was reduced compared to antibacterial activity test of synthesized ZnO nanoparticles. The samples were also incubated for 5 and 120 minutes after dual UV irradiation. As the concentration of immobilized ZnO nanoparticles decreased from 1.0 to 0.05 mg, antibacterial activity increased slightly in *E. coli* (Figure 6A). The incubation time following dual UV irradiation influenced the antibacterial activity for disinfection (Figure 6B–K). Compared with the 5-minute incubation (Figure 6D and F), colonies decreased significantly after the 120-minute incubation of ZnO nanoparticle-immobilized Si

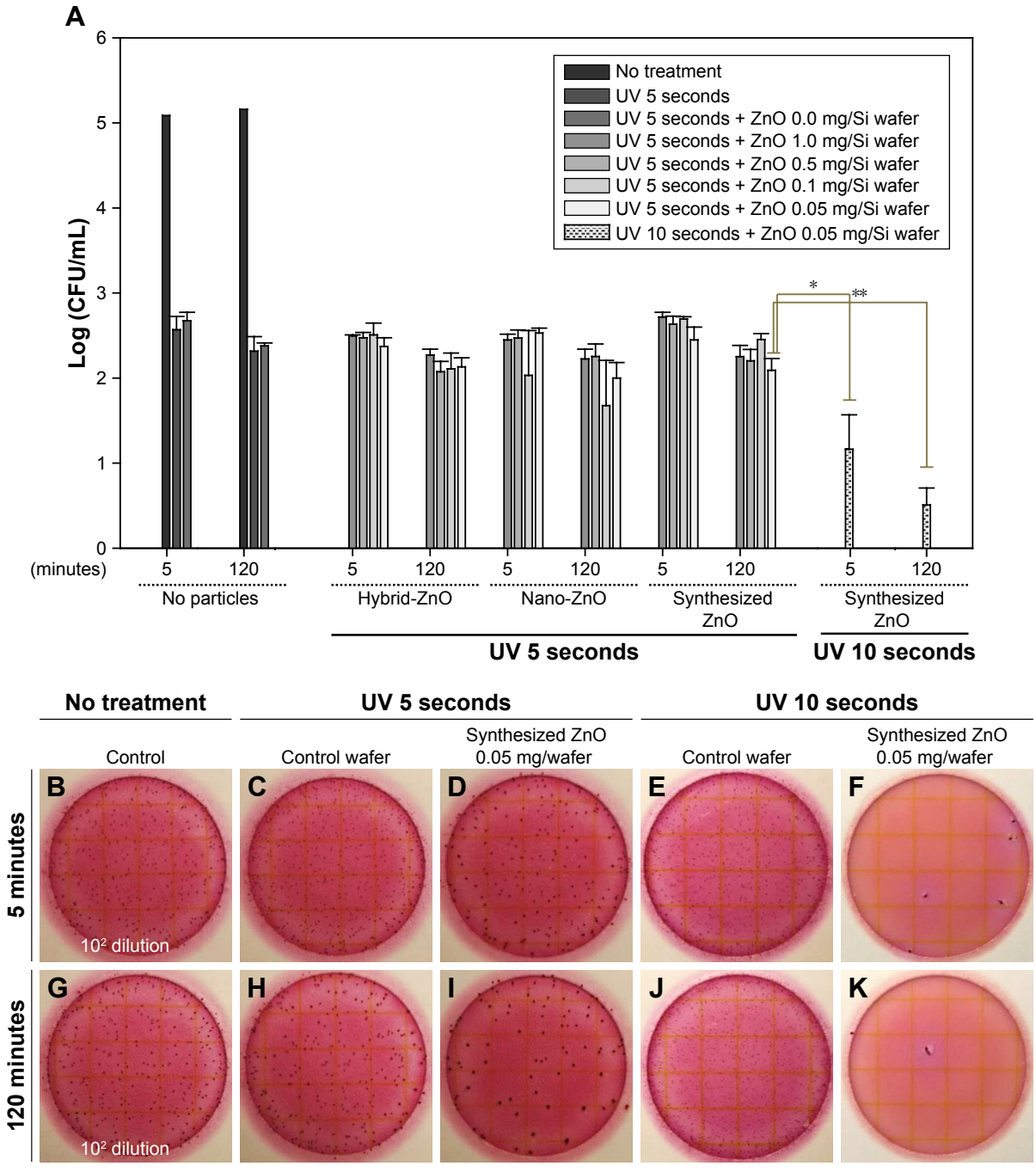

Figure 6 Antibacterial activity of the dual UV-irradiated ZnO nanoparticle network on Si wafer against *Escherichia coli*.
Notes: (**A**) Plots of immobilized ZnO particle concentration vs log(CFU/mL). Representative plate images of (**B** and **G**) *E. coli* colonies (10^2 dilution) with no treatment, and *E. coli* colonies after dual UV irradiation for (**C** and **H**) 5 seconds and (**E** and **J**) 10 seconds and after dual UV-irradiated ZnO nanoparticle network (0.05 mg) treatment – UV irradiation for (**D** and **I**) 5 seconds and (**F** and **K**) 10 seconds; incubation for (**B**–**F**) 5 minutes and (**G**–**K**) 120 minutes. *$P<0.05$ and **$P<0.01$.
Abbreviations: Si, silicon; UV, ultraviolet; ZnO, zinc oxide.

wafers (Figure 6I and K). In the case of dual UV irradiation for 10 seconds, the disinfection potential of immobilized ZnO nanoparticles on the 0.05 mg/Si wafer was enhanced >3 log CFU/mL. Zn ion was not detected in water (Table S1).

Interaction of ZnO nanoparticles with *E. coli*

In terms of antibacterial action mechanisms, ZnO nanoparticles had sorption potential with regard to biomembranes as well as generating ROS, whereas ZnO nanoparticle networks on solid plates mainly produced ROS and reduced the sorption potential. In other words, cellular responses to ROS generation and multiple scattering in self-assembled and multilevel porous ZnO nanoparticle networks can be major events for disinfection against *E. coli* (Figure 7). In biological processes, GO terms for oxidative stress in *E. coli* from EcoCyc are summarized in Table S2. Thiol peroxidase, superoxide dismutase, thioredoxin reductase, and lipid hydroperoxide peroxidase were included in objects annotated in GO terms. Specifically, OxyR (oxyR), a bifunctional sensor for oxidative stress, and protein/nucleic acid deglycase 3 (yajL), a chaperone generated in response to oxidative stress to protect proteins, were GO term members. Although metal ion release from metal oxide nanoparticles is a powerful antimicrobial mechanism, no Zn ion released from ZnO nanoparticles immobilized on Si wafers (0.05 mg/Si wafer) was detected in water after 24-hour incubation.

Cytotoxicity of ZnO nanoparticles in eye and skin cells

Cell viability levels of synthesized ZnO nanoparticles were higher than those of hybrid- and nano-ZnO particles at 0.5–10.0 mg/mL in ARPE-19 and HaCaT cells (Figure 8). Cell viability of ARPE-19 cells (Figure 8A and C) was lower than that of HaCaT cells (Figure 8B and D). The IC50 value in HaCaT cells was highest in synthesized ZnO nanoparticles (6.632 mg/mL), lower in hybrid-ZnO particles (4.476 mg/mL), and lowest in nano-ZnO particles (1.736 mg/mL) after a 48-hour incubation (Figure 8B). In HaCaT cells, low-level synthesized ZnO nanoparticles (0.01–2.0 mg/mL; 0.01–0.5 mg/mL) slightly enhanced cell proliferation levels to 130% after 48 hours (Figure 8B) and 72 hours (Figure 8D) of incubation. No particle shape effects were detected on HaCaT cells at concentrations of 0.01–2.0 mg/mL (Figure S4A–E). These results suggest that synthesized ZnO nanoparticles had low toxicity in eye and skin cells compared with hybrid- and nano-ZnO particles. In addition, eye cells were more susceptible to ZnO particles than skin cells.

Figure 7 Schematic diagram of the antibacterial mechanisms of synthesized ZnO nanoparticles and their self-assembled networks against *Escherichia coli*.
Abbreviations: CB, conduction band; ROS, reactive oxygen species; UV, ultraviolet; VB, valence band; ZnO, zinc oxide.

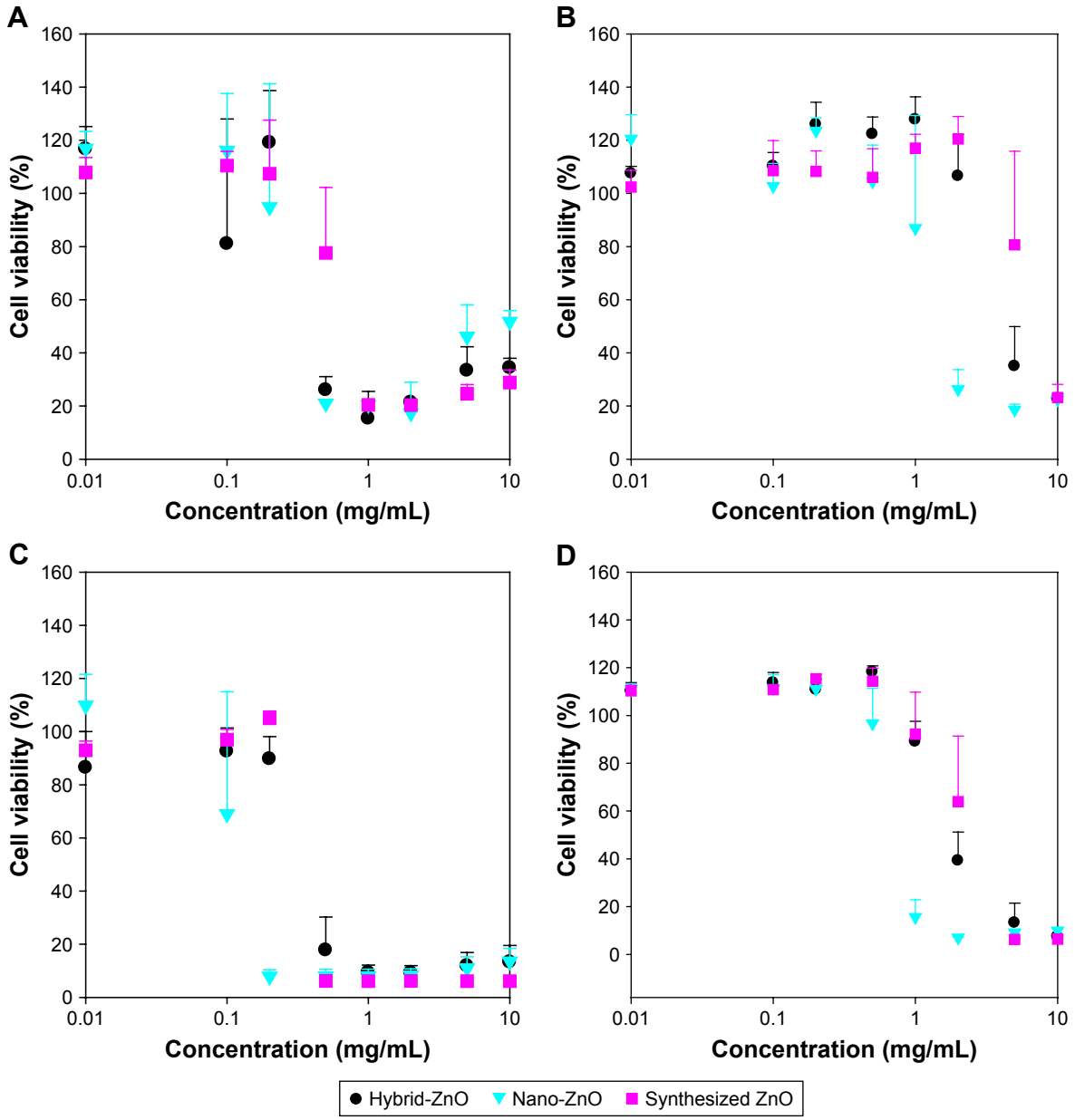

Figure 8 Cytotoxicity of synthesized ZnO nanoparticles in (**A** and **C**) ARPE-19 and (**B** and **D**) HaCaT cells after (**A** and **B**) 48 hours and (**C** and **D**) 72 hours of incubation.
Note: Conventional ZnO particles were used as controls.
Abbreviation: ZnO, zinc oxide.

Phototoxicity of ZnO nanoparticles

ZnO nanoparticle phototoxicity was evaluated in Balb/c 3T3 cells by comparing neutral red uptake after dual UV irradiation of UV-A and UV-C with that after incubation in the dark. Cell viability and the average difference with/without UV irradiation were plotted at 0.001–1.0 mg/mL of synthesized ZnO nanoparticles (Figure 9A and B). The EC50 mean value and EC50 variance value of ZnO nanoparticles after UV irradiation were 0.098 mg/mL, and 0.077 mg/mL, respectively. ZnO nanoparticles at 0.1–1.0 mg/mL showed phototoxicity after dual UV irradiation of UV-A and UV-C (Figure 9C–F). PIF and MPE values were C 14.331 and 0.138, respectively, while PIF and MPE toxicity probability values were 0.900 and 0.745, respectively. On the other hand, conventional hybrid- and nano-ZnO particles affected cell proliferation after dual UV irradiation (Figure S5). Hybrid-ZnO particles induced cell proliferation (~150%) at 0.1–1.0 mg/mL (Figure S5A and C) whereas nano-ZnO particles enhanced cell proliferation (~120%) at 0.001–0.1 mg/mL (Figure S5B and D). PIF and MPE values for hybrid-ZnO particles were C1.000 and −0.193, resulting in toxicity probability values of 0.000. In addition, PIF and MPE values

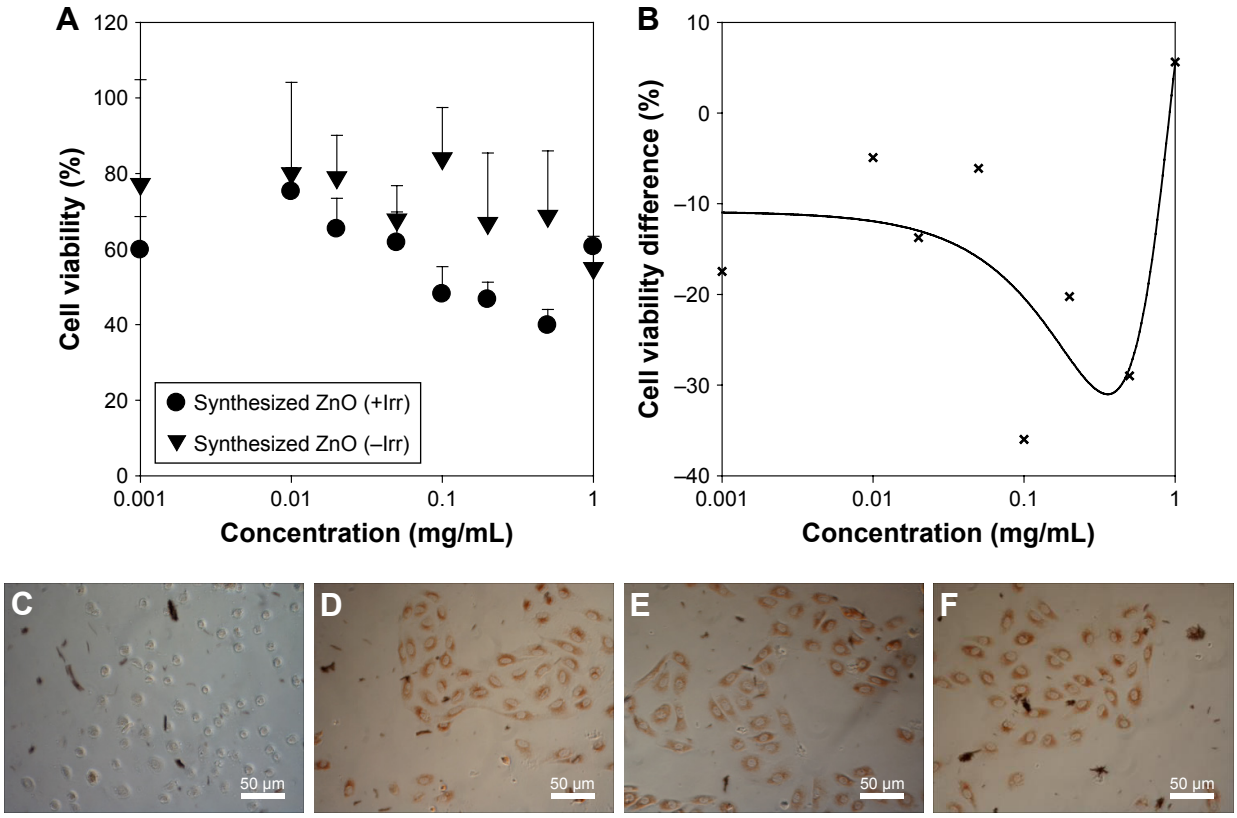

Figure 9 Phototoxicity of synthesized ZnO nanoparticles in Balb/c 3T3 cells: (**A**) cell viability and (**B**) cell viability difference after UV irradiation-based ZnO nanoparticle treatment, and representative images of cells treated with (**C**) 1.0, (**D**) 0.1, (**E**) 0.05, and (**F**) 0 mg/mL ZnO nanoparticles.
Notes: +Irr: with UV irradiation, –Irr: without UV irradiation.
Abbreviations: UV, ultraviolet; ZnO, zinc oxide.

of nano-ZnO particles were C1.000 and –0.288 with toxicity probability values of 0.000. These results suggest that synthesized ZnO nanoparticles are "probably phototoxic" to "phototoxic" as strong photocatalysts under UV irradiation, although they showed low toxicity in skin and eye cells, as mentioned above. Conventional hybrid- and nano-ZnO particles affected cell proliferation levels.

Discussion

ZnO nanoparticles have been extensively studied due to their biocompatibility and similar band gap energy to TiO_2 nanoparticles (3.3 eV) and high electron mobility.[1,2] They have been highlighted as natural alternatives to TiO_2 nanoparticles in various research fields such as photocatalysis and energy storage.[2,3,23] Among the bioapplications of ZnO nanoparticles,[4–13] they have been reported to be photocatalytic antibiotics against bacteria and phages.[5,6,8–13] For general antimicrobial therapy, ZnO nanoparticles also demonstrated therapeutic potential in human pathogens (minimum inhibitory concentration values: 30–80 μg/mL), suggesting the possibility of their use as combination agents with other antibiotics such as cefotaxime and ceftriaxon.[5,8–13] In the present study, the enhanced antibacterial activities of dual UV-irradiated ZnO nanoparticles and multilevel porous networks on Si wafers against *E. coli* have been reported. The physicochemical properties of these nanoparticles and networks were determined using XPS, FE-SEM, FE-TEM, and AFM. ZnO nanoparticle aggregates and arrayed networks had advantages that could maximize antibacterial activity based on the channel structure.[14–21] Specifically, the arrayed networks are essential to minimize unpredicted particle exposure in the environment and to ensure human health.[19,21] Antibacterial activity tests were also performed against *E. coli*. To determine the mechanisms of their antibacterial activity, GO analysis was performed for an *E. coli* database. Low-level cytotoxicity and phototoxicity for synthesized ZnO nanoparticles were also confirmed. Conventional ZnO particles of hybrid-ZnO and nano-ZnO were used as controls.

The physicochemical characteristics of synthesized ZnO nanoparticles were estimated for risk assessment.[16,21] Characterization can provide information on morphology, surface,

UV absorption, nanostructure, and O:Zn ratio related to membrane sorption, ROS generation, and Zn ion release for antimicrobial activity and toxicity.[5,17,22,23] ZnO nanoparticles had sphere shapes with uneven surfaces (<100 nm in diameter) (Figure 1). With regard to morphology and surface, synthesized ZnO nanoparticles were entirely different from conventional ZnO particles (Figure S1), suggesting synthesis method dependence.[5,6,17] The atomic composition of ZnO nanoparticles was also related to material synthesis designs and techniques (Table 1). Binding energy levels of synthesized ZnO nanoparticles in XPS spectra were detected at the same peak positions as conventional ZnO particles (Figure S2). These are comparable to the previously reported results for ZnO nanoparticles.[24] O:Zn ratios and UV absorption levels generally affect the ROS generation potential, which influence antimicrobial activity as well as toxicity.[5,17,21–24]

For macro–mesoporous channels, a synthesized ZnO nanoparticle suspension in hexane naturally formed layered nanostructures on Si wafers after solvent evaporation (Figure 2). EDS technique was used to investigate the characteristics of these engineered three-dimensional structures.[25] An additively manufactured ZnO nanoparticle network by self-assembly was developed in a concentration-dependent manner. A multilevel porous ZnO nanoparticle network formed three-dimensional structures at higher concentrations than seen on the 0.5 mg/Si wafer. Hemisphere- to sphere-shaped ZnO nanoparticle aggregates with mesopores were formed on Si wafers in a low concentration suspension (0.05 mg/Si wafer; Figure 3). Conventional ZnO particles did not produce highly ordered networks of layered structures on Si wafers even at 0.5 mg/Si wafer (Figure S3).

Under dual UV irradiation (Figure 4), we applied synthesized ZnO nanoparticles (Figure 5) and arrayed ZnO nanoparticles on Si wafers (Figure 6) in antibacterial activity testing against *E. coli* in water. Synthesized ZnO nanoparticles had an enhanced activity at 0.05 mg/mL for 5 minutes under dual UV irradiation for 30 seconds compared with conventional ZnO particles. These results suggest that particle–particle and particle–aggregate interactions can enhance the antibacterial activity due to aggregate formation of synthesized ZnO nanoparticles in water compared with the antibacterial activity of hybrid-ZnO particles. Synthesized ZnO nanoparticles also had excellent antibacterial potential under dual UV irradiation in water samples from various facilities. These results are unique compared to those reported by Jin et al using ZnO nanoparticles at 1.0 mg/mL under uncoated dual UV irradiation for 30 seconds.[6] Arrayed ZnO nanoparticles on Si wafers (0.05 mg/Si wafer) showed superior antibacterial activity against *E. coli* (>3 log CFU/mL), even at shortened time of dual UV irradiation from 30 seconds to 10 seconds. Zn ion release was not detected from arrayed ZnO nanoparticles at 0.05 mg/Si wafer (Table S1). However, in the highest concentrations of hybrid- and nano-ZnO particles loaded on Si wafers (1.0 mg/Si wafer), aggregates were easily detached from Si wafers in water. Based on these results, arrayed ZnO nanoparticles on Si wafers showed a superior antibacterial activity compared with free ZnO nanoparticles despite previous studies indicating that the antimicrobial activity of TiO_2 nanoparticles was reduced after immobilization.[16,17,20]

The antibacterial activity of ZnO nanoparticles and arrayed networks on solid plates was described using photocatalysis under dual UV irradiation (Figure 7). The representative action mechanisms of ZnO nanoparticles have been explained by 1) sorption into membranes and consequent membrane disruption and 2) ROS generation.[5,6,22,26] ZnO nanoparticles were highly sorptive on *E. coli* membranes based on hydrophobic and electrostatic interactions. After sorption, they endocytosed or broke down the membrane network and accumulated in *E. coli*.[5,6] ZnO nanoparticles and their aggregates can produce ROS including singlet oxygen ($^1O_2$), hydroxyl radicals ($^{\bullet}OH$), hydrogen peroxide (H_2O_2), and superoxide ($O_2^{-\bullet}$) under UV irradiation.[24] They induce oxidative stress of mitochondria and endoplasmic reticulum dysfunction in *E. coli* resulting in irreversible membrane damage, DNA mutation, and death in *E. coli*. Zn ion was not released from nanoparticles or nanoparticle networks, suggesting that nanoparticle antibacterial potential was not mediated by Zn ions.

Photocatalytic activity can also be improved by the multiple scattering induced by arrayed ZnO nanoparticles in three-dimensional structure networks.[27–29] Macro–mesoporous channel-based structure formation and multiple scattering in the nanoparticle networks were affected by physicochemical characteristics such as particle size and specific surface area. The zeta potential of ZnO nanoparticles was also related to aggregation formation in self-assembled nanostructure-induced photocatalysis enhancement. In general, ZnO nanoparticles showed positive zeta potential values at neutral to slightly basic pH.[30] The bimodal channels from interparticle interactions enhanced mass transfer in the networks. Compared to synthesized ZnO nanoparticles and conventional ZnO particles (hybrid- and nano-ZnOs), arrayed ZnO nanoparticles on Si wafers showed enhanced antibacterial activity without bacterial regrowth after treatment.

Using GO terms in a biology model, the interactions between ZnO nanoparticles and internal proteins in *E. coli*

were investigated. GO terms with members are listed in Table S2. Using immobilized ZnO particles on Si wafers, the photocatalyst function of ZnO nanoparticles was focused on antibacterial potential more than Zn ion release and sorption to biomembrane in *E. coli*. GO terms with related proteins can explain the mechanism of action of the internal response of *E. coli* to oxidative stress; related protein expression can be modified for enhanced therapeutic effects.[22–26] Proteins involved in oxidative stress on *E. coli*, specifically DNA-binding transcriptional dual regulator OxyR (oxyR) and protein/nucleic acid deglycase 3 (yajL), were searched in EcoCyc.[22] OxyR and YajL act as "a bifunctional regulatory protein sensor for oxidative stress" and "a chaperone, protecting proteins in response to oxidative stress", respectively. In other words, OxyR in *E. coli* activates a hydrogen peroxide-inducible gene regulon as a hydrogen peroxide sensor for induction of a defense signal.[29,31] YajL also has a repair catalysis function to deglycate Maillard adducts between protein amino groups/nucleotides and glyoxal reactive carbonyl groups.[32,33] They protect against environmental oxidative stress in *E. coli*.

Nanoparticle toxicity is an important issue in nanoparticle development for various applications. In this study, techniques of damage-free repeated cell rinsing and reference subtraction were used to remove all artifacts. Synthesized ZnO nanoparticles showed lower cytotoxicity in HaCaT (Figure S4) and ARPE-19 cells than conventional hybrid- and nano-ZnO particles (Figure 8). The slight cell proliferation potential of ZnO nanoparticles at 0.5–200 μg/mL has already been reported in HaCaT after 24-hour incubation.[34] IC50 values of ZnO nanoparticles (synthesized ZnO, 6.632 mg/mL; hybrid-ZnO, 4.476 mg/mL; nano-ZnO, 1.736 mg/mL) were much higher than previously reported ZnO nanoparticle results. Vinardell et al reported the IC50 values of ZnO (50 nm) and ZnO (100 nm) nanoparticles to be around 50 and 40 μg/mL, respectively, in HaCaT cells after a 48-hour incubation period.[35] Genç et al also reported that nanoscale to microscale ZnO particles showed lower toxicity in HaCaT cells than ZnO nanoparticles (<100 nm in diameter) with/without UV-A and UV-B.[36] Compared to TiO_2 nanoparticle toxicity, TiO_2 nanoparticles had an autophagic effect on HaCaT cells in a dose-dependent manner even at noncytotoxic levels.[37] Synthesized ZnO nanoparticles were phototoxic under dual UV irradiation (UV-A and UV-C; Figure 9) compared with conventional ZnO particles on Balb/c 3T3 cells (Figure S5).

Overall, ZnO nanoparticles and their immobilized network on Si wafers had excellent disinfection potential as photocatalysts under dual UV irradiation. Sophisticated three-dimensional ZnO structures formed with multi-level porosity via self-assembly. They showed superior antibacterial activity against *E. coli* at >3 log CFU/mL without environmental or health exposure risks. Although synthesized ZnO nanoparticles were phototoxic, they were less toxic in skin and eye cells than conventional ZnO particles. These results suggest that ZnO nanoparticles and self-assembled ZnO nanoparticle networks on solid plates can be implemented in the dual UV irradiation systems as effective and safe photocatalytic antibiotics. Their application can also be extended to highly pathogenic microorganisms for enhanced disinfection, suggesting their promising potential in near-future disinfection systems for clinical and industrial uses.

Conclusion

ZnO nanoparticles were synthesized and immobilized onto the solid plates (Si wafers). Three-dimensional ZnO nanoparticle networks formed hierarchically porous nanostructures on Si wafers via self-assembly after solvent evaporation. Synthesized ZnO nanoparticles and arrayed ZnO nanoparticle networks on solid plates had excellent antibacterial activity against *E. coli* under dual UV irradiation at >3 log CFU/mL. Immobilized forms of arrayed ZnO nanoparticles showed superior antibacterial activity compared with synthesized ZnO nanoparticles. Membrane sorption and ROS generation without Zn ion release were included in the main antibacterial mechanisms of action. In immobilized ZnO nanoparticle networks on solid plates, multiple scattering and bimodal channel structures could enhance the antibacterial activity against *E. coli* despite the reduction of membrane sorption potential. With regard to cellular response, OxyR and YajL proteins were searched in GO term members related to oxidative stress in *E. coli*. Synthesized ZnO nanoparticles had lower toxicity in skin and eye cells than conventional ZnO particles; however, they were phototoxic. These results suggest that dual UV-irradiated ZnO nanoparticles and self-assembled nanoparticle networks on solid plates have antibacterial effects against *E. coli*. In addition, they show considerable promise as photocatalytic nanoantibiotics for use in near future disinfection systems with industrial and clinical applications.

Acknowledgments

This work was partially supported by the Korea Ministry of Environment (MOE) as part of "The advancement of scientific research and technological development in environmental science program (2016000140006)". Prof

Jong-Wha Jung and Minjun Kim, PhD candidate, kindly provided ZnO nanoparticles.

Disclosure

The authors report no conflicts of interest in this work.

References

1. Solanki PR, Kaushik A, Agrawal VV, Malhotra BD. Nanostructured metal oxide-based biosensors. *NPG Asia Mater*. 2011;3(1):17–24.
2. Yu X, Marks TJ, Facchetti A. Metal oxides for optoelectronic applications. *Nat Mater*. 2016;15(4):383–396.
3. Abd-El-Aziz AS, Agatemor C, Etkin N. Antimicrobial resistance challenged with metal-based antimicrobial macromolecules. *Biomaterials*. 2017;118:27–50.
4. Allahverdiyev AM, Abamor ES, Bagirova M, Rafailovich M. Antimicrobial effects of $TiO_{(2)}$ and $Ag_{(2)}O$ nanoparticles against drug-resistant bacteria and *Leishmania* parasites. *Future Microbiol*. 2011;6(8):933–940.
5. Amna S, Shahrom M, Azman S. Review on zinc oxide nanoparticles: antibacterial activity and toxicity mechanism. *Nano-Micro Lett*. 2015;7(3):219–242.
6. Jin SE, Hwang W, Lee HJ, Jin HE. Dual UV irradiation-based metal oxide nanoparticles for enhanced antimicrobial activity in *Escherichia coli* and M13 bacteriophage. *Int J Nanomedicine*. 2017;12:8057–8070.
7. Jin SE, Ahn HS, Kim JH, et al. Boiling method-based zinc oxide nanorods for enhancement of adipose-derived stem cell proliferation. *Tissue Eng Part C Methods*. 2016;22(9):847–855.
8. Mirhosseini M, Firouzabadi FB. Antibacterial activity of zinc oxide nanoparticle suspensions on food-borne pathogens. *Int J Dairy Technol*. 2013;66(2):291–295.
9. Liu J, Rojas-Andrade MD, Chata G, et al. Photo-enhanced antibacterial activity of ZnO/graphene quantum dot nanocomposites. *Nanoscale*. 2018;10(1):158–166.
10. Raja A, Ashokkumar S, Pavithra Marthandam R, et al. Eco-friendly preparation of zinc oxide nanoparticles using *Tabernaemontana divaricata* and its photocatalytic and antimicrobial activity. *J Photochem Photobiol B*. 2018;181:53–58.
11. Bhande RM, Khobragade CN, Mane RS, Bhande S. Enhanced synergism of antibiotics with zinc oxide nanoparticles against extended spectrum β-lactamase producers implicated in urinary tract infections. *J Nanopart Res*. 2013;15(1):1413.
12. Aditya A, Chattopadhyay S, Jha D, Gautam HK, Maiti S, Ganguli M. Zinc oxide nanoparticles dispersed in ionic liquids show high antimicrobial efficacy to skin-specific bacteria. *ACS Appl Mater Interfaces*. 2018;10(18):15401–15411.
13. Kadiyala U, Turali-Emre ES, Bahng JH, Kotov NA, VanEpps JS. Unexpected insights into antibacterial activity of zinc oxide nanoparticles against methicillin resistant *Staphylococcus aureus* (MRSA). *Nanoscale*. 2018;10(10):4927–4939.
14. Alrousan DM, Dunlop PS, McMurray TA, Byrne JA. Photocatalytic inactivation of *E. coli* in surface water using immobilised nanoparticle TiO_2 films. *Water Res*. 2009;43(1):47–54.
15. Ede S, Hafner L, Dunlop P, Byrne J, Will G. Photocatalytic disinfection of bacterial pollutants using suspended and immobilized TiO_2 powders. *Photochem Photobiol*. 2012;88(3):728–735.
16. Zheng X, Shen G, Wang C, et al. Bio-inspired Murray materials for mass transfer and activity. *Nat Commun*. 2017;8:14921.
17. Baranwal A, Srivastava A, Kumar P, Bajpai VK, Maurya PK, Chandra P. Prospects of nanostructure materials and their composites as antimicrobial agents. *Front Microbiol*. 2018;9:422.
18. Avci C, Imaz I, Carné-Sánchez A, et al. Self-assembly of polyhedral metal–organic framework particles into three-dimensional ordered superstructures. *Nat Chem*. 2017;10(1):78–84.
19. Zhang J, Li Y, Zhang X, Yang B. Colloidal self-assembly meets nanofabrication: from two-dimensional colloidal crystals to nanostructure arrays. *Adv Mater*. 2010;22(38):4249–4269.
20. Schneider D, Mehlhorn D, Zeigermann P, Kärger J, Valiullin R. Transport properties of hierarchical micro-mesoporous materials. *Chem Soc Rev*. 2016;45(12):3439–3467.
21. Yu L, Zheng-yi F, Bao-lian S. Hierarchically structured porous materials for energy conversion and storage. *Adv Funct Mater*. 2012;22(22):4634–4667.
22. Keseler IM, Mackie A, Santos-Zavaleta A, et al. The EcoCyc database: reflecting new knowledge about *Escherichia coli* K-12. *Nucleic Acids Res*. 2017;45(D1):D543–D550.
23. Boken J, Soni SK, Kumar D. Microfluidic synthesis of nanoparticles and their biosensing applications. *Crit Rev Anal Chem*. 2016;46(6):538–561.
24. Yuan G, Xiang J, Jin H, Wu L, Jin Y, Zhao Y. Anchoring ZnO nanoparticles in nitrogen-doped graphene sheets as a high-performance anode material for lithium-ion batteries. *Materials (Basel)*. 2018;11(1):96.
25. Nagarajan S, Arumugam Kuppusamy K. Extracellular synthesis of zinc oxide nanoparticle using seaweeds of Gulf of Mannar, India. *J Nanobiotechnology*. 2013;11(1):39.
26. Dizaj SM, Lotfipour F, Barzegar-Jalali M, Zarrintan MH, Adibkia K. Antimicrobial activity of the metals and metal oxide nanoparticles. *Mater Sci Eng C*. 2014;44:278–284.
27. Yang XY, Chen LH, Li Y, Rooke JC, Sanchez C, Su BL. Hierarchically porous materials: synthesis strategies and structure design. *Chem Soc Rev*. 2017;46(2):481–558.
28. Parlett CM, Wilson K, Lee AF. Hierarchical porous materials: catalytic applications. *Chem Soc Rev*. 2013;42(9):3876–3893.
29. Christman MF, Storz G, Ames BN. OxyR, a positive regulator of hydrogen peroxide-inducible genes in *Escherichia coli* and *Salmonella typhimurium*, is homologous to a family of bacterial regulatory proteins. *Proc Natl Acad Sci U S A*. 1989;86(10):3484–3488.
30. Marsalek R. Particle size and zeta potential of ZnO. *APCBEE Procedia*. 2014;9:13–17.
31. Storz G, Tartaglia LA. OxyR: a regulator of antioxidant genes. *J Nutr*. 1992;122(3 Suppl):627–630.
32. Le HT, Gautier V, Kthiri F, et al. YajL, prokaryotic homolog of parkinsonism-associated protein DJ-1, functions as a covalent chaperone for thiol proteome. *J Biol Chem*. 2012;287(8):5861–5870.
33. Abdallah J, Mihoub M, Gautier V, Richarme G. The DJ-1 superfamily members YhbO and yajL from *Escherichia coli* repair proteins from glycation by methylglyoxal and glyoxal. *Biochem Biophys Res Commun*. 2016;470(2):282–286.
34. Gao F, Ma N, Zhou H, et al. Zinc oxide nanoparticles-induced epigenetic change and G2/M arrest are associated with apoptosis in human epidermal keratinocytes. *Int J Nanomedicine*. 2016;11:3859–3874.
35. Vinardell M, Llanas H, Marics L, Mitjans M. In vitro comparative skin irritation induced by nano and non-nano zinc oxide. *Nanomaterials (Basel)*. 2017;7(3):56.
36. Genç H, Barutca B, Koparal AT, Özöğüt U, Şahin Y, Suvacı E. Biocompatibility of designed MicNo-ZnO particles: cytotoxicity, genotoxicity and phototoxicity in human skin keratinocyte cells. *Toxicol In Vitro*. 2018;47:238–248.
37. Lopes VR, Loitto V, Audinot J-N, Bayat N, Gutleb AC, Cristobal S. Dose-dependent autophagic effect of titanium dioxide nanoparticles in human HaCaT cells at non-cytotoxic levels. *J Nanobiotechnology*. 2016;14(1):22.